AIAA JOURNAL
Vol. 38, No. 10, October 2000

Effects of Combustion and Shock Impingement on Supersonic Film Cooling by Hydrogen

Kenichi Takita* and Goro Masuya†
Tohoku University, Sendai 980-8579, Japan

Supersonic film cooling with H_2 coolant was numerically investigated by considering the combustion of the coolant and the impingement of the shock wave. The influence of temperature fluctuation was included in calculating chemical rate constants. The combustion region was formed apart from the wall, and there was little heat release from the flame. Therefore, the combustion of H_2 had only a weak influence on the characteristics of the film cooling. The location of ignition moved upstream considerably due to the temperature fluctuations. However, the movement decreased the cooling efficiency very slightly. In addition, the effect of shock impingement on the film cooling by reactive H_2 was almost the same as that of nonreactive N_2 with the same coolant injection Mach number.

Nomenclature

A = Jacobian matrix
a = sonic velocity, m/s
C = mole fraction
c = constants
d = height of coolant injector, m
$\boldsymbol{E}$ = vectors of convective fluxes in the ξ direction
$\boldsymbol{E}_v$ = vectors of viscous fluxes in the ξ direction
$\boldsymbol{F}$ = vectors of convective fluxes in the η direction
$\boldsymbol{F}_v$ = vectors of viscous fluxes in the η direction
f = damping functions or mass fraction
f_c = film cooling efficiency
J = Jacobian
K = turbulent kinetic energy, m^2/s^2
K_T = temperature fluctuation, K^2
k_l = reaction rate not including temperature fluctuation
k_t = reaction rate including temperature fluctuation
L_0 = reference length, =0.05 m
M = Mach number
P = probability density
P_K = production term of turbulent kinetic energy defined in Eq. (2)
P_T = production term of temperature variance
p = pressure, MPa
Re_0 = reference Reynolds number
R_t = turbulent Reynolds number defined by Eq. (6)
R_y = turbulent Reynolds number defined by Eq. (6)
$\boldsymbol{S}$ = vectors of source terms
T = temperature, K
t = time, s
U = contravariant velocity, m/s
$\boldsymbol{U}$ = vectors of conserved variables
u = velocity in x direction, m/s
v = velocity in y direction, m/s
x, y = space coordinates, m
γ = stoichiometric coefficient
δ = boundary layer thickness, m
ε = dissipation rate of K, m^2/s^3
ε_τ = dissipation rate of temperature variance, K^2/s
λ = thermal conductivity, J/(m s K)
μ = viscosity, kg/(m s)
ν = kinematic viscosity, m^2/s
ξ, η = generalized curvilinear coordinates
ρ = density, kg/m^3
σ = ratios of turbulent transport coefficient
ω_i = mass production rate of i species, $kg/(m^3\ s)$

Subscripts

aw = adiabatic wall
b = backward reaction
c = coolant
e = efficient region of film cooling
f = forward reaction
m = main flow
t = turbulent
w = wall
0 = stagnation

Superscripts

L = left-hand side of cell interface
R = right-hand side of cell interface
$()'$ = fluctuation or left-hand side of stoichiometric equation
$()''$ = right-hand side of stoichiometric equation
$(\bar{})$ = mean value

Presented as Paper 99-2146 at the AIAA/ASME/SAE/ASEE 35th Joint Propulsion Conference, Los Angeles, CA, 20–23 June 1999; received 26 July 1999; revision received 22 November 1999; accepted for publication 23 March 2000.

*Assistant Professor, Department of Aeronautics and Space Engineering, Aramaki; takita@cc.mech.tohoku.ac.jp. Member AIAA.

†Professor, Department of Aeronautics and Space Engineering, Aramaki. Member AIAA.

Introduction

THERMAL protection of an engine wall exposed to high temperature burnt gas is indispensable for the development of the scramjet engine for an aerospace plane. Film cooling, especially in combination with regenerative cooling, is a promising way to achieve such protection.[1] Thus, recently, supersonic film cooling has been intensively investigated numerically[2,3] and experimentally[4–9] from various viewpoints, following the fundamental experiments[10,11] a few decades ago. When a combination of film cooling and regenerative cooling is employed, the total temperature of the film coolant flow becomes much higher than its storage temperature. H_2 fuel is widely considered to be an appropriate coolant for use in the system of a space plane. In the case of H_2 coolant, however, the possibility of combustion of high temperature H_2 must be taken into consideration. In their experiments on supersonic film cooling, Bass et al.[9] observed that the combustion of H_2 occurred at an average temperature lower than the autoignition temperature. They hypothesized that large temperature fluctuations caused such combustion. However, there have been few studies on the effects of combustion of coolant on the film cooling efficiency under the condition of large temperature fluctuations. Even the modeling of numerical schemes for such flow is still under development.

Obviously, there is a possibility that the formation of the combustion region changes the flowfield and the mixing rate between the coolant flow and the main flow. Different characteristics of

H_2 coolant from nonreactive coolant such as N_2 may thus appear in the performance of film cooling. In particular, the effects of impingements of a shock wave and an expansion wave on the combustion region of H_2 film becomes important because such wave impingements cause changes in the static temperature, the static pressure, and the intensity of turbulence around the site of impingement. In our previous study,[3] the effect of shock wave impingement was numerically investigated and the results were compared with experimental data.[6,7] However, the reaction of a coolant was not considered.

Therefore, the purpose of this study was to numerically analyze the combustion phenomena of H_2 coolant in the flowfield of supersonic film cooling and to investigate its influence on the cooling characteristics, considering both the temperature fluctuation and the shock wave impingement. Of course, the analysis of combustion with large temperature fluctuation is indispensable for the development of the combustor of the scramjet engine.[12–16]

Governing Equations and Numerical Method

The two-dimensional compressible Navier–Stokes equations in the generalized curvilinear coordinate for multispecies were considered to be the governing equations

$$\frac{\partial \boldsymbol{U}}{\partial t} + \frac{\partial \boldsymbol{E}}{\partial \xi} + \frac{\partial \boldsymbol{F}}{\partial \eta} = \frac{\partial \boldsymbol{E}_v}{\partial \xi} + \frac{\partial \boldsymbol{F}_v}{\partial \eta} + \boldsymbol{S} \tag{1}$$

Detailed descriptions of vectors of convective, viscous, and source terms are described in Refs. 17 and 18. The K-ε low-Reynolds-number turbulent model by Lam and Bremhorst,[19] in which eddy viscosity does not become zero when flow separation occurs, was used. The field equations for K and are written as

$$\boldsymbol{U}_{K\varepsilon} = J\begin{bmatrix}\rho K\\ \rho\varepsilon\end{bmatrix}, \qquad \boldsymbol{E}_{K\varepsilon} = J\begin{bmatrix}\rho K U_\xi\\ \rho\varepsilon U_\xi\end{bmatrix}$$

$$\boldsymbol{E}_{vK\varepsilon} = \frac{J}{Re_0}\begin{bmatrix}\left(\mu + \dfrac{\mu_t}{\sigma_K}\right)\xi_i \dfrac{\partial K}{\partial x_i}\\ \left(\mu + \dfrac{\mu_t}{\sigma_\varepsilon}\right)\xi_i \dfrac{\partial \varepsilon}{\partial x_i}\end{bmatrix}$$

$$\boldsymbol{S}_{K\varepsilon} = J\begin{bmatrix}P_K - \rho\varepsilon\left(1 + M_t^2\right)\\ (f_1 c_1 P_K - f_2 c_2 \rho\varepsilon)\dfrac{\varepsilon}{K}\end{bmatrix}$$

$$P_K = \left\{\mu_t\left[\left(\frac{\partial u_i}{\partial x_j} + \frac{\partial u_j}{\partial x_i}\right) - \frac{2}{3}\delta_{ij}\frac{\partial u_k}{\partial x_k}\right] - \frac{2}{3}\delta_{ij}\rho K\right\}\frac{\partial u_i}{\partial x_j} \tag{2}$$

The eddy viscosity is calculated from

$$\mu_t = c_\mu f_\mu (\rho K^2/\varepsilon) \tag{3}$$

The closure coefficients, such as damping functions, are as follows:

$$f_\mu = [1 - \exp(-0.0165 R_y)]^2 (1 + 20.5/R_t) \tag{4}$$

$$f_1 = 1 + (0.05/f_\mu)^3, \qquad f_2 = 1 - \exp\left(-R_t^2\right) \tag{5}$$

$$R_t = K^2/\nu\varepsilon, \qquad R_y = (\sqrt{K}\cdot y)/\nu \tag{6}$$

$$c_1 = 1.44, \qquad c_2 = 1.92, \qquad c_\mu = 0.09$$

$$\sigma_K = 1.0, \qquad \sigma_\varepsilon = 1.3 \tag{7}$$

Sarkar's correction[20] for the compressibility effect was applied to the source term in the governing equation of K.

To calculate the temperature fluctuation, conservation equations of temperature variance (K_T) and its dissipation rate (ε_T) were added to the governing equations. The field equations[21,22] for K_T and ε_T are written as

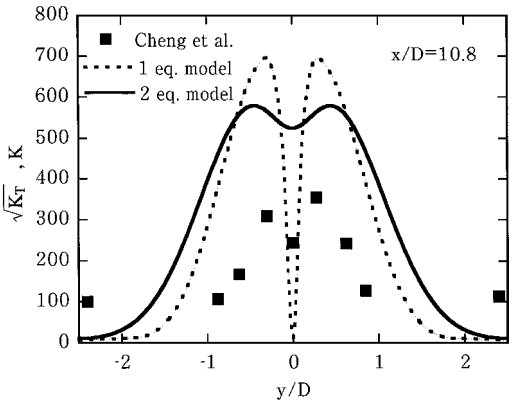

Fig. 1 Comparison of temperature fluctuations between experiment and calculation for case of H_2 jet in vitiated airflow.

$$\boldsymbol{U}_{K\varepsilon(T)} = J\begin{bmatrix}\rho K_T\\ \rho\varepsilon_T\end{bmatrix}, \qquad \boldsymbol{E}_{K\varepsilon(T)} = J\begin{bmatrix}\rho K_T U_\xi\\ \rho\varepsilon_T U_\xi\end{bmatrix}$$

$$\boldsymbol{E}_{vK\varepsilon(T)} = \frac{J}{Re_0}\begin{bmatrix}\left(\lambda + \dfrac{\mu_t}{\sigma_{K_T}}\right)\xi_i \dfrac{\partial K_T}{\partial x_i}\\ \left(\lambda + \dfrac{\mu_t}{\sigma_{\varepsilon_T}}\right)\xi_i \dfrac{\partial \varepsilon_T}{\partial x_i}\end{bmatrix}$$

$$\boldsymbol{S}_{K\varepsilon(T)} = J\begin{bmatrix}2c_{K_T1}P_T - 2c_{K_T2}\rho\varepsilon_T\\ \dfrac{\varepsilon_T}{K_T}\left(C_{\varepsilon_T 1}P_T - c_{\varepsilon_T 2}\rho\varepsilon_T\right) + \dfrac{\varepsilon_T}{K}\left(C_{\varepsilon_T 3}P_K - c_{\varepsilon_T 4}\rho\varepsilon\right)\end{bmatrix}$$

$$K_T = T'T', \qquad P_T = \frac{\mu_t}{\sigma_{K_T}}\left(\frac{\partial T}{\partial x_i}\right)^2 \tag{8}$$

$$c_{K_T1} = 2.70, \quad c_{K_T2} = 0.05, \quad c_{\varepsilon_T1} = 1.80, \quad c_{\varepsilon_T2} = 2.20$$
$$c_{\varepsilon_T3} = 0.72, \quad c_{\varepsilon_T4} = 0.80, \quad \sigma_{K_T} = 1.0, \quad \sigma_{\varepsilon_T} = 1.0 \tag{9}$$

In Eqs. (8) and (9), the temperature variance is coupled with the turbulent kinetic energy. To validate these models, a comparison with the experiment of a supersonic H_2 jet by Cheng et al.,[23] was conducted. The flowfield of the experiment was constituted from pure H_2 jet with 2.36 mm diam (D) in vitiated coairflow (O_2 20%, N_2 54.4%, and H_2O 25.5%). Static temperatures and Mach numbers were 545 K and 1.0 for the H_2 jet, and 1250 K and 2.0 for the vitiated airflow, respectively. Figure 1 shows distributions of temperature fluctuation in vertical direction to the flow at $X/D = 10.8$ from the exit of the nozzle. The comparison between a one-equation model[12] and a two-equation model for temperature fluctuation are also shown in Fig. 1. The advantage of the two-equation model is obviously demonstrated in Fig. 1. The qualitative behavior of the temperature fluctuation calculated from the two-equation model was in agreement with the experimental result, for example, a little decrease in the temperature fluctuation around the centerline of the jet, though the maximum value was overestimated about 50%. This overestimation would result in reduction of the ignition distance in a mixing layer. However, the location of ignition points had very small effect on the characteristics of the film cooling as shown in the following results.

The 3rd-order MUSCL TVD scheme was used for the finite difference of convective terms:

$$\boldsymbol{E}_{j+\frac{1}{2}} = \left[\boldsymbol{E}\left(\boldsymbol{U}^R_{j+\frac{1}{2}}\right) + \boldsymbol{E}\left(\boldsymbol{U}^R_{j+\frac{1}{2}}\right) - \left|\boldsymbol{A}\left(\boldsymbol{U}^R_{j+\frac{1}{2}}, \boldsymbol{U}^L_{j+\frac{1}{2}}\right)\right| \times \left(\boldsymbol{U}^R_{j+\frac{1}{2}} - \boldsymbol{U}^L_{j+\frac{1}{2}}\right)\right] \Big/ 2.0$$

$$\boldsymbol{A} = \frac{\partial \boldsymbol{E}}{\partial \boldsymbol{U}} \tag{10}$$

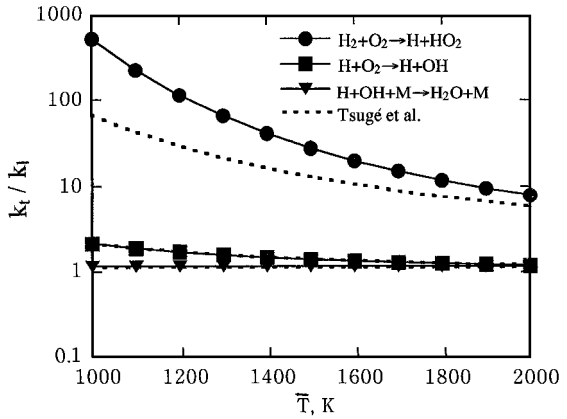

Fig. 2 Reaction rates with temperature fluctuations for different initial temperatures ($T' = 0.2T$).

The H_2/O_2 combustion model by Stahl and Warnatz[24] constituted from nine species (H_2, O_2, H_2O, O, H, OH, HO_2, H_2O_2, and N_2) and 37 elementary reactions was used in the present calculation. N_2 was assumed to be an inert gas, and its reactions were omitted.

The mean production rates of species and the mean reaction rates were calculated by considering the temperature fluctuations. The following relations obtained by Tsugé et al.[25] were used in order to save computational time.

$$\overline{(\dot{\omega}_i)_j} = M_i(\gamma''_{ji} - \gamma'_{ji}) \cdot \left(\overline{k_{fj}} \prod_{k=1}^{n} C_k^{\gamma'_{jk}} - \overline{k_{bj}} \prod_{k=1}^{n} C_k^{\gamma''_{jk}} \right) \tag{11}$$

$$\overline{k_{fj}} = \frac{1}{2}\left\{ k_{fj}\left(\bar{T} + \sqrt{\overline{K_T}}\right) + k_{fj}\left(\bar{T} - \sqrt{\overline{K_T}}\right) \right\}$$

$$\overline{k_{bj}} = \frac{1}{2}\left\{ k_{bj}\left(\bar{T} + \sqrt{\overline{K_T}}\right) + k_{bj}\left(\bar{T} - \sqrt{\overline{K_T}}\right) \right\} \tag{12}$$

These equations were compared with the reaction rates obtained by using PDF of temperature assumed to have a Gaussian distribution[12,13,15,16] as follows:

$$\overline{k_{fj}} = \int_{\bar{T}-2\sqrt{\overline{K_T}}}^{\bar{T}+2\sqrt{\overline{K_T}}} k_{fj} P(T)\, \mathrm{d}T$$

$$\overline{k_{bj}} = \int_{\bar{T}-2\sqrt{\overline{K_T}}}^{\bar{T}+2\sqrt{\overline{K_T}}} k_{bj} P(T)\, \mathrm{d}T \tag{13}$$

$$P(T) = \frac{1}{\sqrt{2\pi \overline{K_T}}} \exp\left[\frac{-(T-\bar{T})^2}{2\overline{K_T}} \right] \tag{14}$$

Figure 2 shows a comparison of the amplitude of reaction rates with temperature fluctuation for different mean temperature calculated by Eqs. (12) and (13). Calculations were conducted for three representative reactions. The results show good agreement for the chain branching reaction ($H + O_2 \rightarrow OH + H$) and the chain termination reaction ($H + OH + M \rightarrow H_2O + M$), though the rate of the chain initiation reaction ($H_2 + O_2 \rightarrow H + HO_2$) is underestimated. This underestimation sometimes lengthens the ignition distances of reactive mixing layers.

Results and Discussion

Comparisons with experimental results[6,7] were made in a previous paper[3] for the case of N_2 coolant. In the present paper, our main concerns were the three effects of combustion of a coolant, temperature fluctuation, and shock wave impingement on the characteristics of H_2 film cooling.

Effect of Combustion

The flowfield of supersonic film cooling with the combustion of the coolant was investigated in the simple configuration shown in Fig. 3 to clarify its effect. The main flow consisted of burnt gas (N_2, O_2, and H_2O), and the coolant flow was pure H_2. The height and the length of the computational domain were 18 and 75 mm, respectively, and the height of the coolant injector was 4 mm. The film cooling efficiency in the case of no reaction is maintained at almost unity in this region. For the sake of simplicity, the thickness of the splitter plate of the injector was not considered. The computational grid had 151 ×181 grid points. Nonslip and adiabatic conditions were given for the lower wall boundary, and boundary layer profiles deduced from the $\frac{1}{7}$th power law were assumed for both flows at the entrance. The thickness of the boundary layers were given as 1 mm for the coolant flow and 5 mm for the main flow. A reflected wave from the upper wall was weak and not important in the flowfield; therefore, the slip condition was applied to the upper wall.

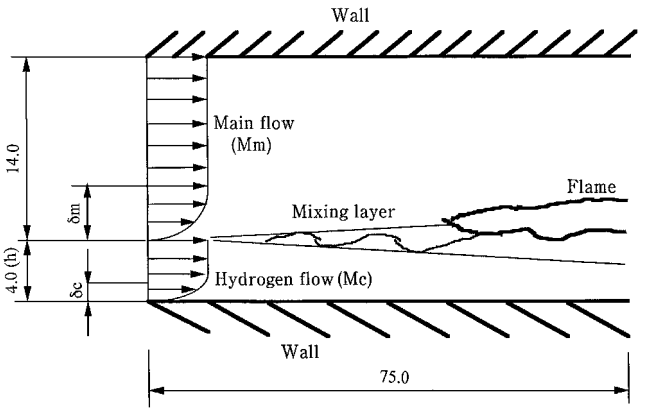

Fig. 3 Schematic of flow configuration.

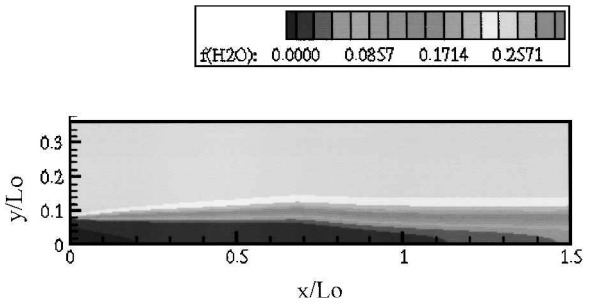

Fig. 4 Contour of H_2O mass fraction (mass fraction of O_2 in main flow is 5%).

Dependence on Mass Fraction of Oxygen in Main Flow

The O_2 mass fraction in the main flow basically depends on the fuel equivalence ratio and the combustion efficiency of the engine. If the combustion efficiency is 100% and the equivalence ratio is unity or larger, there is no possibility of combustion reaction for the coolant. Therefore, the mass fraction of O_2 in the main flow becomes an important factor, and thus its effect on the combustion of H_2 coolant was calculated first. The mass fractions of H_2O and N_2 in the entrance flow with no O_2 were 0.25 and 0.75, respectively. The three cases in which O_2 (5, 10, and 20%) was added to the main flow were investigated. The conditions of the coolant flow were same for all cases, and then O_2 was simply replaced by N_2 in order to negate the change of the mixing rate by the change of the sonic velocity of the main flow.

Figure 4 shows a contour of the H_2O mass fraction for a typical case in which the flow conditions are $T_m = 1250$ K (total temperature is about 2100 K), $p_m = 0.1$ MPa, $M_m = 2.0$ for the main flow, and $T_c = 400$ K (total temperature is about 500 K), $p_c = 0.1$ MPa, $M_c = 1.1$ for the coolant flow. The mass fraction of O_2 in the main flow is 5%. Combustion did not occur for these conditions, as shown in Fig. 4, which is a contour of mass fraction of H_2O. The H_2O that was a constituent of the main flow diffused monotonically toward the wall. The mixing of the main flow and the coolant flow gradually proceeded downstream, the same as in the flowfield of the nonreactive coolant, and the wall temperature was maintained at the adiabatic recovery temperature of the coolant flow. The maximum

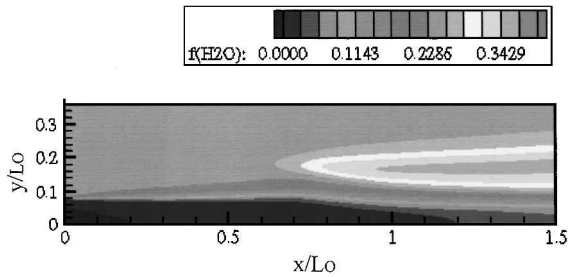

a) H_2O mass fraction

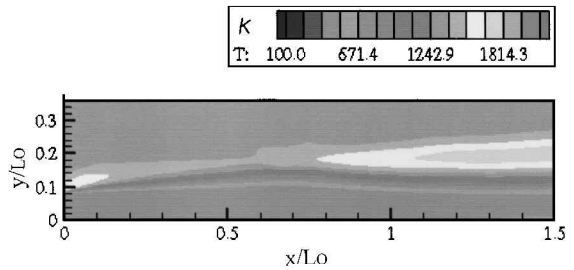

b) Temperature

Fig. 5 Contours of variables in flowfield (mass fraction of O_2 in main flow is 10%).

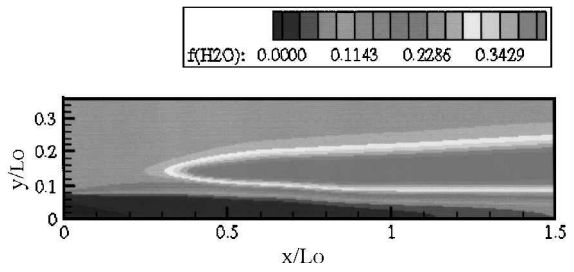

a) H_2O mass fraction

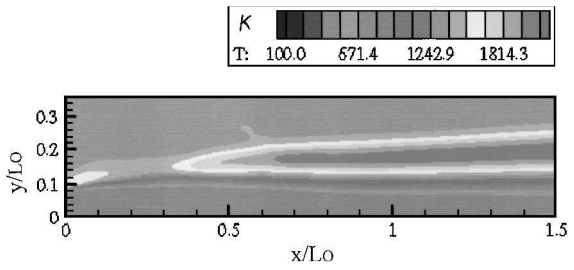

b) Temperature

Fig. 6 Contours of variables in flowfield (mass fraction of O_2 in main flow is 20%).

mass fraction of the OH radical was $O(10^{-6})$ at the right boundary of Fig. 3. It was reported in Refs. 5 and 9 that the nondimensional effective length (x_e/d) of the film cooling by H_2, which had large heat capacity was much larger than that of air or N_2 for the same mass flow ratio of a main flow and a coolant flow.

Figure 5 shows contours of the H_2O mass fraction and the temperature for the case in which the mass fraction of O_2 is 10%. The maximum mass fraction of the OH is about 7.0×10^{-3} at the right boundary. Combustion obviously occurred in Fig. 5, but strong heat release in the combustion region did not appear. If the O_2 in the main flow perfectly reacted with H_2, the mass fraction of the H_2O exceeded 0.4. It is obvious from the contour of the temperature that the combustion region gradually moved away from the wall as it traveled downstream. Pressure waves generated by the combustion were not observed on either side of the coolant flow or the main flow, indicating that heat release was slight and that the Mach number of the coolant flow injected with supersonic velocity ($M_c = 1.1$) became subsonic downstream. Deceleration of the coolant flow was observed regardless of the occurrence of combustion.

Figure 6 shows contours of the H_2O mass fraction and the temperature for the case in which the mass fraction of O_2 is 20%. This

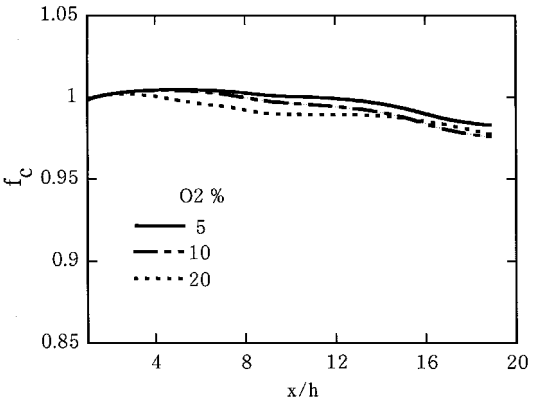

Fig. 7 Film cooling efficiencies for different mass fraction of O_2 in main flow.

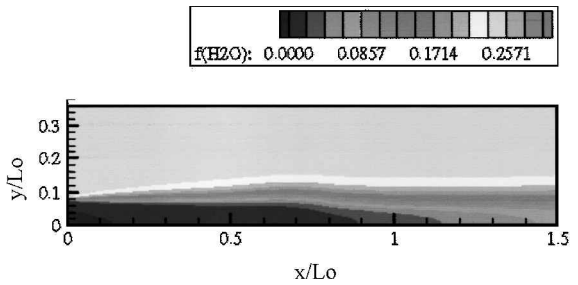

Fig. 8 Contour of H_2O mass fraction (mass fraction of O_2 is 5% in main flow and T_c = 500 K).

mass fraction of O_2 is almost the same as that of the flow that has not reacted (23%). The ignition point went considerably upstream and the ignition distance was in inverse proportion to the mass fraction of O_2 in the main flow. However, the combustion region downstream did not spread in the transverse direction toward the wall, because the mixing did not proceed. No strong pressure wave was formed by the combustion, the same as in the case of 10% O_2. The maximum temperature was obtained at $x/d = 15.0$, and it was about 100 K higher than the stagnation temperature of the main flow. After all, large changes in the flowfield did not appear as the result of the combustion of the coolant, which, if observed, was always weak and occurred apart from the wall.

The film cooling efficiencies (f_c) for the three O_2 mole fractions are shown in Fig. 7. The definition of the cooling efficiency is as follows:

$$f_c = \frac{T_{aw} - T_{0m}}{T_{0c} - T_{0m}} \tag{15}$$

It is obvious from Fig. 7 that the effect of the combustion of the coolant on the cooling efficiency was very small, though the cooling efficiency slightly decreased in proportion to the degree of combustion. In the region where the cooling efficiency was maintained at almost unity, the coolant film near the wall was not hurt by its combustion.

Effect of Total Temperature of Coolant Flow

The combination of film cooling and regenerative cooling results in high total temperature of the coolant flow.[1] Therefore, the effect of the total temperature of the coolant flow must be investigated. In the case of a nonreactive coolant such as N_2, the increase in the total temperature results in improvement of the cooling characteristics because of the increase in the injection velocity for the same total pressure.

Figure 8 shows a contour of the H_2O mass fraction for the case in which $T_c = 500$ K (total temperature is about 600 K) and the other conditions are the same as in the case of Fig. 4. No strong reaction occurred and the maximum OH mass fraction was $O(10^{-6})$. These results indicate that the combustion characteristics depend mainly on the flow conditions of the main flow where the flame is always formed, and the effect of the change in the total temperature of

the coolant flow becomes weak. The same tendency was previously obtained in the analysis of the characteristics of a counterflow diffusion flame in a supersonic airflow.[26,27]

Effects of Temperature Fluctuations

Change in Temperature Fluctuation in Flowfield of Film Cooling

Bass et al.[9] reported that the ignition of H_2 coolant occurred at a temperature lower than the autoignition temperature due to large temperature fluctuations in the flowfield. Therefore, considerations of temperature fluctuations are required for the analysis. However, studies on film cooling in the past have not mentioned such effects.

To grasp the fundamental behavior of the temperature fluctuations in the flowfield of the film cooling, calculations were conducted for the same flow conditions as those of Kanda's experiments[8,9] in which both the main flow and the coolant flow were N_2, and the total temperature ratio was 1.2. The configuration of the flowfield is shown in Fig. 9. The height of the computational domain is 5 cm and that of the coolant injector is 4 mm. The shock generator, with a deflection angle of 3, 6, or 8 deg, is attached to the upper wall. The splitter plate between the main flow and the coolant flow was assumed to be 1.5 mm in height. At the left boundary, the inflow conditions are given as follows: the total pressure and the Mach number of the main flow are 1.35 MPa (p_{0m}) and 2.35 (M_m), respectively, and those of the coolant flow are 200 kPa (p_{0c}) and 1.0 (M_c). Nonslip and adiabatic conditions are given for the wall boundary, and boundary layer profiles deduced from the $\frac{1}{7}$th power law for both flows are assumed. Also, total temperature of the coolant flow was set at 230 K (T_{0c}) as a constant. The film cooling efficiencies and the wall pressure for both the case of shock impingement and that of no shock impingement have already been compared with experimental results, and good agreement was obtained in Ref. 3. Figure 10, for example, shows a comparison of the cooling efficiencies for different angles of the shock generator, which was not investigated in the previous work.[3] In Fig. 10, the horizontal axis was rearranged by using the mass flux ratio in order to consider differences of the coolant species; the approximate relation obtained in the numerical study by O'Connor et al.[2] is also shown. The dependence of the cooling efficiency on the strength of the impinging shock wave also agreed well with the experimental result.

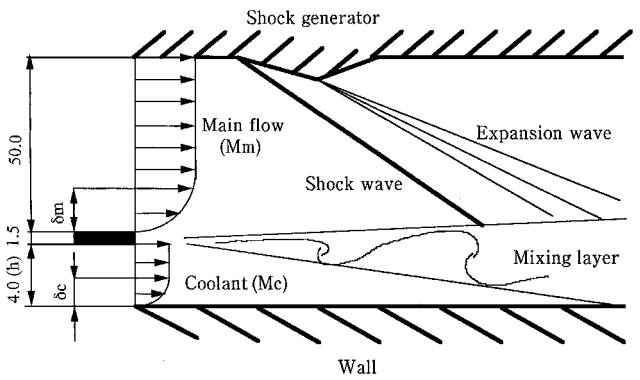

Fig. 9 Flowfield of experiment by Kanda et al.[6,7]

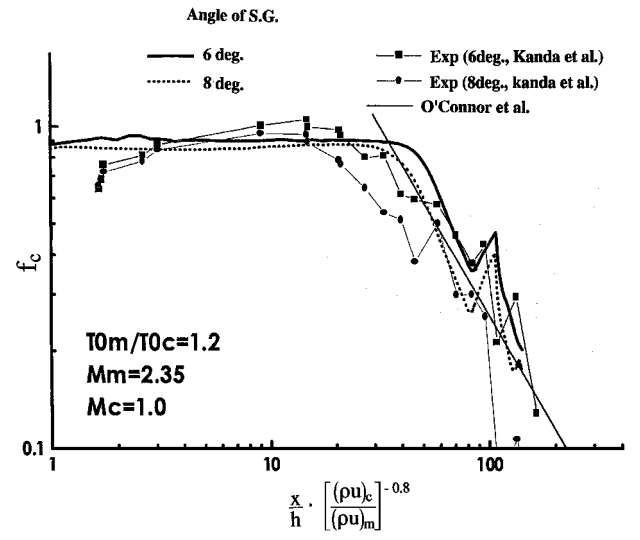

Fig. 10 Film cooling efficiencies for different strengths of shock wave.

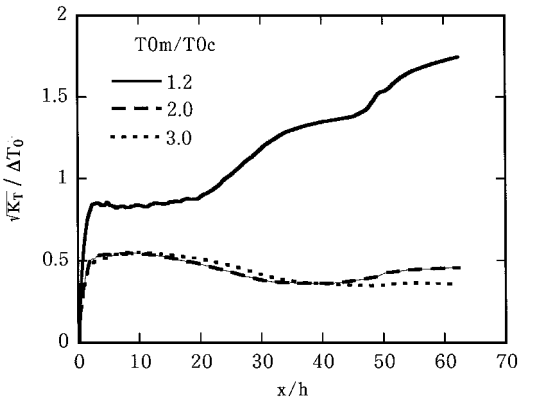

Fig. 11 Change in nondimensional temperature fluctuations for different total temperature ratios.

Figure 11 shows distributions of nondimensional temperature fluctuation for three total temperature ratios. The square root of the temperature variance was nondimensionalized by the difference in total temperatures between the main flow and the coolant flow as one of the parameters for the arrangement. Results for the low total temperature ratio ($T_{0m}/T_{0c} = 1.2$), which agreed with conditions of most of the past experiments,[4–7] showed a different tendency with regard to the high total temperature ratio. The temperature fluctuation gradually increased with distance downstream, and was higher than that in the case of the high total temperature ratio for the whole range, though the difference between the total temperatures was very small (about 50 K). On the other hand, in the case of the high total temperature ratio, temperature fluctuations decreased gradually in the downstream direction. The maximum values of the temperature fluctuation were almost the same for two high temperature ratios. These results showed that estimations of the temperature fluctuation and its effect on the cooling efficiency could not be attained by experiments of low total temperature ratio, in particular, the case in which the static temperature of the coolant was higher than that of the main flow (so-called film heating). Establishment and validation of a method for analysis of such fluctuations in a compressible flow are needed.

In addition, the dependence of fluctuations on the strength of the shock wave was investigated. Temperature fluctuations slightly increased with the strength of the shock wave around the position of shock impingement and were gradually amplified downstream. However, the degree of the increase was not so large. The reason for this weak dependence on the shock strength was considered to be that the change in the static temperature by shock impingement was small. After all, the temperature fluctuations depended mainly on the difference in the static temperatures of the main flow and the coolant flow.

Case of Reactive Coolant

The effect of temperature fluctuations for the H_2 coolant was investigated in this section. The same flow conditions as those shown in Fig. 4 (O_2 mass fraction was 10%) were chosen for the test case. Figure 12 shows contours of the H_2O mass fraction, the OH mass fraction, and the temperature fluctuation. The temperature fluctuation was nondimensionalized by the difference of total temperatures between the main flow and the coolant flow. Compared with the case in which temperature fluctuations were not included, the location of ignition moved considerably upstream. However, the combustion region did not spread downstream toward the wall, and the heat release from the region and the maximum temperature did not change much. The tendency in Fig. 12 was almost the same as that of the flowfield in the case that the mass fraction of O_2 in the main flow increased as seen in Fig. 5. The large value of temperature

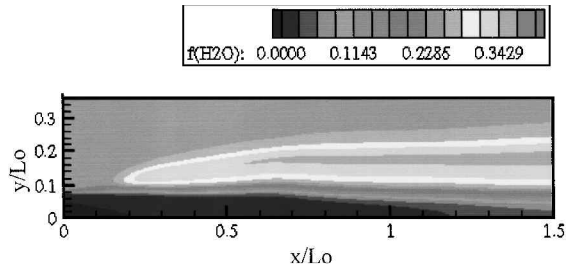

a) H_2O mass fraction

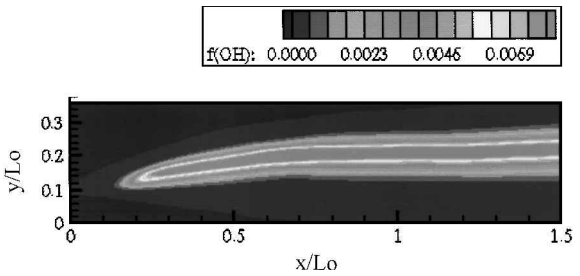

b) OH mass fraction

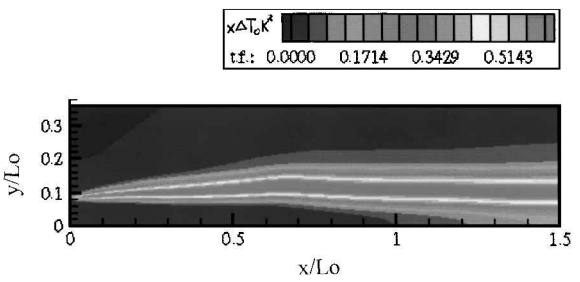

c) Temperature fluctuation

Fig. 12 Contours of variables in flowfield with considering temperature fluctuation (mass fraction of O_2 in main flow is 10%).

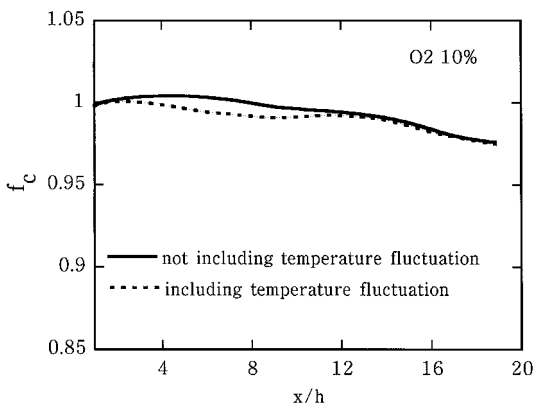

Fig. 13 Comparison of film cooling efficiencies with and without temperature fluctuation.

fluctuation was found not along the flame surface but in the mixing layer. If there had been a large heat release from the flame, a large temperature fluctuation would have been produced there due to the large temperature difference. Figure 13 shows the change of the cooling efficiency when temperature fluctuations are considered. It is obvious from the figure that the difference was slight.

Effect of Shock Wave Impingement on hydrogen Coolant Flow

The present authors investigated the effects of shock wave impingement on a coolant flow of N_2 in a previous study.[3] In that study, the results showed that the decrease in the cooling efficiency due to shock impingement was mainly the result of the decrease in local Mach number as reported by Kanda et al.,[6] and the mixing rate between the main flow and the coolant flow was not so changed by the shock impingement. These results obtained for nonreactive coolant

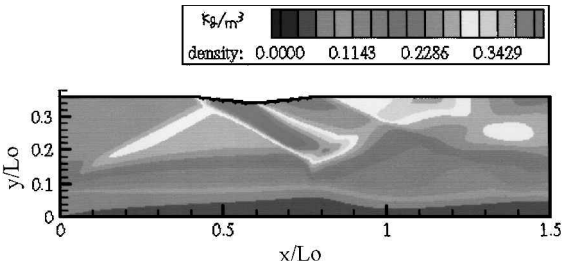

a) Density

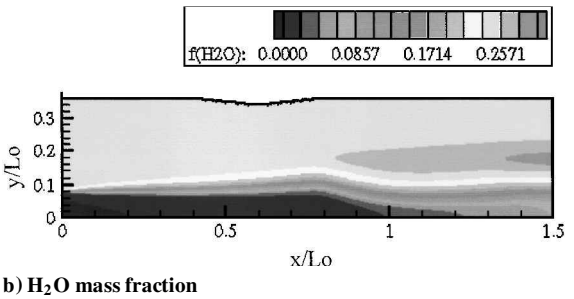

b) H_2O mass fraction

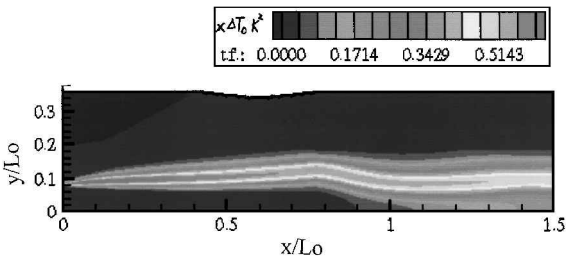

c) Temperature fluctuation

Fig. 14 Contours of variables in flowfield for case of shock impingement of 6 deg.

are fundamentally applicable to a reactive coolant. If a reaction does not occur in the flowfield, no difference between a nonreactive coolant and a reactive coolant exists. However, there is a possibility of the enhancement of the reaction and mixing of the coolant due to increases in the local static temperature, the static pressure, and the intensity of turbulence at the site of the shock impingement.

Therefore, the effect of shock impingement was investigated for the same flow conditions as in Fig. 3 with the shock impingement from the shock generator of 6 deg. When the Mach number of the main flow was 2.0, the shock wave moved and a steady state was not obtained due to the strong interaction with subsonic region of the coolant flow, which was formed downstream of the impingement site. Calculations were then conducted for the case of $M_c = 2.5$ and $T_c = 1250$ K (total temperature was about 2600 K). Figure 14 shows contours of the density, the H_2O mass fraction, and the temperature fluctuation. As seen in these figures, no strong reaction occurred as the result of the shock impingement for this Mach number, though the maximum value of the OH mass fraction became slightly larger than in the case without shock impingement. The increases in the local static pressure and the static temperature were not large, and the degree of mixing was also not changed at the site where the shock impinged. The behavior of the mixing layer was almost the same as that of the N_2 coolant in Ref. 3.

Next, calculation using reaction rates with temperature fluctuation was conducted for the same flow conditions as those in Fig. 14. Figure 15 shows contours of the density, the H_2O mass fraction, the OH mass fraction, and the temperature fluctuation. The area where H_2O was formed became larger than that of Fig. 14, and local enhancement of the reaction appeared behind the site of the shock impingement. However, the basic structure of the flowfield did not change. Figure 16 shows a comparison of the cooling efficiencies for the above two cases and for the case of no shock impingement. The effect of shock impingement on cooling efficiency was greater than those of the occurrence of combustion and the location of the flame. As a result, the effect of the shock impingement

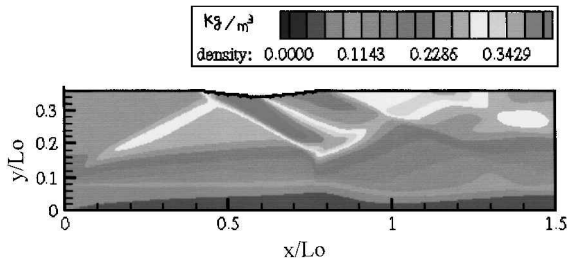

a) Density

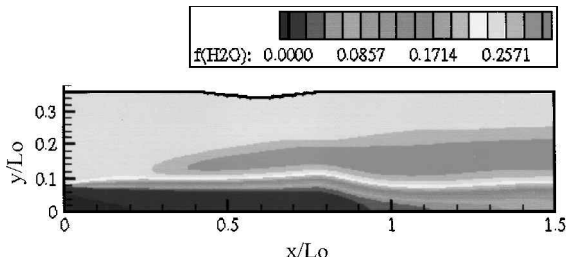

b) H_2O mass fraction

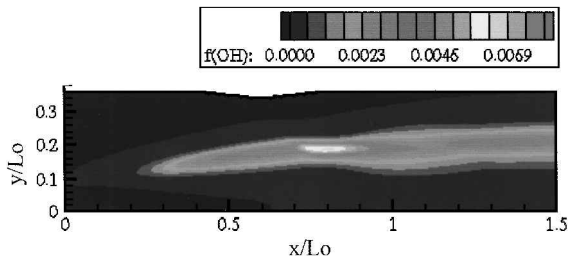

c) OH mass fraction

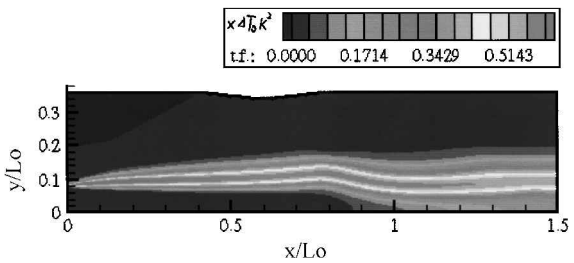

d) Temperature fluctuation

Fig. 15 Contours of variables in flowfield for case that shock impingement and temperature fluctuation are considered.

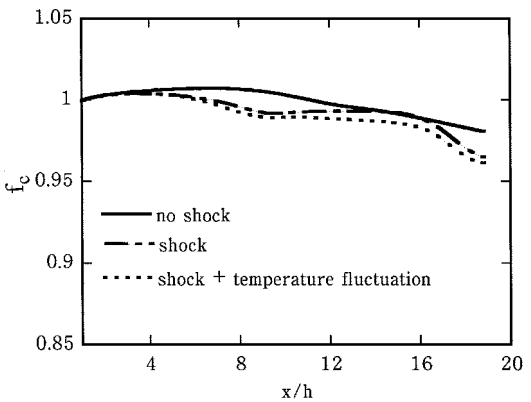

Fig. 16 Comparison of film cooling efficiencies with and without shock impingement.

did not make any difference in the flowfields between the reactive and nonreactive coolants.

Conclusions

The effects of combustion and shock impingement on supersonic film cooling by H_2 coolant were numerically investigated. The following results were obtained:

1) The effect of the combustion of the coolant on the flowfield was weak, and the flame was always formed apart from the wall. Strong heat release and a pressure wave generated by the combustion were not observed.

2) The increase in total temperature of the coolant did not result in any considerable change in the behavior of the coolant flow. The combustion characteristics depend mainly on the conditions of the main flow side.

3) The ignition location moved upstream considerably for H_2 coolant when the temperature fluctuation was included in the calculation, but the transverse spread of combustion region toward the wall did not increase downstream, and the heat release from the combustion was slight. As a result, the film cooling efficiency did not change much.

4) No large difference of the effect of the shock impingement on the film cooling between H_2 and nonreactive coolant appeared.

5) The change of temperature fluctuation for low total temperature ratio of the main flow and the coolant flow showed different behavior from one for high total temperature ratio. Therefore, the formation of temperature fluctuation for high temperature ratio could not be estimated from experiments of low total temperature ratio.

Acknowledgment

The authors are grateful to Takanori Kobari for his help.

References

[1]Kanda, T., Masuya, G., Ono, F., and Wakamatsu, Y., "Effect of Film Cooling/Regenerative Cooling on Scramjet Engine Performances," *Journal of Propulsion and Power*, Vol. 10, No. 5, 1994, pp. 618–624.

[2]O'Connor, J. P., and Haji-Sheikh, A., "Numerical Study of Film Cooling in Supersonic Flow," *AIAA Journal*, Vol. 30, No. 10, 1992, pp. 2426–2433.

[3]Takita, K., and Masuya, G., "The Effects of Shock Impingement on Supersonic Film Cooling," *Journal of Spacecrafts and Rockets*, Vol. 34, No. 4, 1999, pp. 602–604.

[4]Juhany, K. A., and Hunt, M. L., "Flowfield Measurements in Supersonic Film Cooling Including the Effect of Shock-Wave Interaction," *AIAA Journal*, Vol. 32, No. 3, 1994, pp. 578–585.

[5]Juhany, K. A., Hunt, M. L., and Sivo, J. M., "Influence of Injectant Mach Number and Temperature on Supersonic Film Cooling," *Journal of Thermophysics and Heat Transfer*, Vol. 8, No. 1, 1994, pp. 59–67.

[6]Kanda, T., Ono, F., Takahashi, M., Saito, T., and Wakamatsu, Y., "Experimental Studies of Supersonic Film Cooling with Shock Wave Interaction," *AIAA Journal*, Vol. 34, No. 2, 1996, pp. 265–271.

[7]Kanda, T., and Ono, F., "Experimental Studies of Supersonic Film Cooling Shock Wave Interaction (2)," *Journal of Thermophysics and Heat Transfer*, Vol. 11, No. 4, 1997, pp. 590–593.

[8]Aupoix, B., Mignosi, A., Viala, S., Bouvier, F., and Gaillard, R., "Experimental and Numerical Study of Supersonic Film Cooling," *AIAA Journal*, Vol. 36, No. 6, 1998, pp. 915–923.

[9]Bass, R., Hardin, L., Rodgers, R., and Ernst, R., "Supersonic Film Cooling," AIAA Paper 90-5239, 1990.

[10]Goldstein, R. J., Eckert, E. R. G., Tsou, F. K., and Haji-Seikh, A., "Film Cooling with Air and Helium Injection Through a Rearward-Facing Slot Into a Supersonic Air Flow," *AIAA Journal*, Vol. 4, No. 6, 1966, pp. 981–985.

[11]Parthasarathy, K., and Zakkay, V., "An Experimental Investigation of Turbulent Slot Injection at Mach 6," *AIAA Journal*, Vol. 8, No. 7, 1970, pp. 1302–1307.

[12]Gaffney, Jr., R. L., White, J. A., Girimaji, S. S., and Drummond, J. P., "Modeling Turbulent/Chemistry Interactions Using Assumed PDF Methods," AIAA Paper 92-3638, 1992.

[13]Baurle, R. A., Alexopoulos, G. A., and Hassan, A., "Assumed Joint Probability Density Function Approach for Supersonic Turbulent Combustion," *Journal of Propulsion and Power*, Vol. 10, No. 4, 1994, pp. 473–484.

[14]Hsu, A. T., Tsai, Y.-L. P., and Raju, M. S., "Probability Density Function Approach for Compressible Turbulent Reacting Flows," *AIAA Journal*, Vol. 32, No. 7, 1994, pp. 1407–1415.

[15]Baurle, R. A., Alexopoulos, G. A., and Hassan, H. A., "Modeling of Supersonic Turbulent Combustion Using Assumed Probability Density Functions," *Journal of Propulsion and Power*, Vol. 10, No. 6, 1994, pp. 777–786.

[16]Baurle, R. A., Hsu, A. T., and Hassan, H. A., "Assumed and Evolution Probability Density Functions in Supersonic Turbulent Combustion Calculations," *Journal of Propulsion and Power*, Vol. 11, No. 6, 1995, pp. 1132–1138.

[17]Takita, K., and Niioka, T., "Counterflow Diffusion Flame of Methane and Methane/Hydrogen Mixed Fuel in Supersonic Flow," *Journal of Propulsion and Power*, Vol. 13, No. 2, 1997, pp. 233–238.

[18]Takita, K., "Film Cooling Effect of Hydrogen on Cylinder in Supersonic Airflow," *Journal of Spacecraft and Rockets*, Vol. 34, No. 3, 1997, pp. 285–289.

[19]Lam, C. K. G., and Bremhorst, K., "A Modified Form of the k-e Model for Predicting Wall Turbulence," *Journal of Fluid Engineering*, Vol. 103, No. 3, 1981, pp. 456–460.

[20]Sarkar, S., Erlebacher, G., Hussaini, M. Y., and Kress, H. O., "The Analysis and Modeling of Dilatational Terms in Compressible Turbulence," *Journal of Fluid Mechanics*, Vol. 227, 1991, pp. 473–493.

[21]Jones, W. P., and Musonge, P., *Proceedings of the 4th Symposium on Turbulent Shear Flows*, 1983.

[22]Mizobuchi, Y., and Ogawa, S., "Computation of Hydrogen Injection Into Supersonic Air Flow," *Proceedings of the 14th Symposium on Computational Gas Dynamics of Aeroplanes*, 1997, pp. 165–170 (in Japanese).

[23]Cheng, T., Wehmeyer, J., Pitz, R., Jarrett, O., Jr., and Northam, G., "Finite-Rate Chemistry Effects in a Mach 2 Reacting Flow," AIAA Paper 91-2320, 1991.

[24]Stahl, G., and Warnatz, J., "Numerical Investigation of Time-Dependent Properties and Extinction of Strained Methane- and Propane-Air Flamelets," *Combustion and Flame*, Vol. 85, 1991, pp. 285–299.

[25]Tsugé, S., and Sagara, K., "Arrhenius Law in Turbulent Media and an Equivalent Tunnel Effect," *Combustion Science and Technology*, Vol. 18, 1978, pp. 179–189.

[26]Takita, K., "Analytical Study on Counterflow Diffusion Flame in Supersonic Flow," Ph.D Dissertation, Dept. of Aeronautics and Space Engineering, Tohoku Univ., Aramaki, Sendai, Japan, 1996.

[27]Takita, K., and Niioka, T., "Numerical Simulation of a Counterflow Diffusion Flame in Supersonic Airflow," *Proceedings of the 26th Symposium (International) on Combustion*, Combustion Inst., Pittsburgh, PA, 1996, pp. 2877–2883.

S. K. Aggarwal
Associate Editor